



29 **1. Introduction**

30 Evapotranspiration is the principle process in defining mass and energy relationship in the
31 surrounding hydrosphere (Allen et al., 2007a,b; Cruz-Blanco, et al., 2014). The consumptive use
32 of irrigational water in agriculture is the fundamental component of a balanced estimation of
33 evapotranspiration (Bastiaanssen et al., 1998; Cammalleri and Ciraolo, 2013).

34 The concept of water use efficacy is basically depending on the reliable estimation of
35 evapotranspiration and surface water evaporation (Berengena and Gavilán, 2005; Elhag et al.,
36 2011). Weather and wind conditions induce a regional and seasonal variation of
37 evapotranspiration estimation (Hanson, 1991; Cristobal and Anderson 2012).

38 Conventional techniques of field scale evapotranspiration estimations are fairly achieved epically
39 over homogenous surfaces using ordinary techniques: lysimeter systems, Eddy Covariance (EC)
40 and Bowen Ratio (BR). Nevertheless, conventional methods of evapotranspiration estimations
41 are incapable of fulfilling the quest of regional evapotranspiration estimation specifically in
42 harsh climatic conditions (Gavilán et al., 2006; Ghilain et al., 2011). Therefore, remote sensing
43 evapotranspiration models are adequate techniques to bring satisfactory estimates (Allen et al.,
44 2007a,b; De Bruin et al., 2010).

45 Remote sensing evapotranspiration models are numerous. Several algorithms are already in
46 practice with different complexity levels to estimate fairly evapotranspiration based on different
47 climatic conditions and land use variability (Elhag et al., 2011; Espadafor et al., 2011; Cristobal,
48 and Anderson 2012).

49 Based on several scholarly work of Roerink et al., (2000); Su, (2002); Crago et al., (2005);
50 Cha´vez et al., (2005); Loheide and Gorelick, (2005); Allen et al., (2007a,b); Ghilain et al.,



51 (2011); Psilovikos and Elhag (2013) on remote sensing evapotranspiration based algorithms,
52 there are principally two types of evapotranspiration estimation concepts on terrestrial surfaces.

53 The first concept is to use the surface reflectance in different visible (VIS), near-infrared (NIR)
54 and even extended to Thermal Infrared (TIR) portions of the electromagnetic spectrum to
55 rationalize the Surface Energy Balance (SEB). The other concept it to use vegetation indices
56 derived from canopy reflectance to conceptualize remotely sensed crop coefficient (K_{cr}).

57 Gourd truth data collection exercised at less than one-meter canopy height, in which all related
58 surfaces fluxes and atmospheric surface variables of the vegetation cover takes place in arid
59 environment takes place (Beljaars and Holtslag 1991; Zwart and Bastiaanssen, 2004). Based on
60 Brutsaert (1991, 1999), Monin-Obukhov Similarity (MOS) and Bulk Atmospheric Boundary
61 Layer (ABL) functions were calculated. Brutsaert (1999) suggested sets of criteria estimate MOS
62 or ABL if it scaled down appropriately for a given circumstances. Brutsaert criteria are valid
63 only for unstable conditions.

64 Therefore, van den Hurk and Holtslag (1995) adjusted and validated Brutsaert criteria using
65 atmospheric surface layer scaling according to Brutsaert (1982) to be used in stable conditions.
66 Generic estimation of Surface Albedo for vegetated land covers is based on the red (R) and NIR
67 band reflectance (Brest and Goward 1987) model.

68 The aim of the current study is to monitor turbulent heat fluxes in Wadi Ad Dawasir to estimate
69 the daily evapotranspiration rate and relative evaporation ratio using AATSR and MERIS
70 sensors. The final step is to identify the regression coefficient between the estimated
71 evapotranspiration's rates and the actual ground truth data.

72



73 **2. Materials and methods**

74 **2.1. Study area**

75 The study area, Wadi Ad Dawasir town is located on the plateau of Najd at Lat 44° 43' and Lon
76 20° 29'; about 300 km south of the capital city Riyadh. This study area comprised of gravelly
77 tableland disconnected by insignificant sandy oases and isolated mountain bundles. Across the
78 Arabian Peninsula as a whole, the tableland slopes toward the east from an elevation of 1,360
79 meters in the west to 750 meters at its easternmost limit. Wadi Ad Dawasir and Wadi ar
80 Rummah the most important pattern of the ancient riverbeds remains in the study area. Wadi Ad
81 Dawasir and Najran regions are the major irrigation water abstraction from Al-Wajid aquifer.
82 Agriculture in Wadi Ad Dawasir area consists of technically highly developed farm enterprises
83 that operate modern pivot irrigation system. The size of center pivot ranges from 30 ha to 60 ha
84 with farms managing hundreds of them with the corresponding number of wells. The main crop
85 grown in winter is wheat and occasionally potatoes, tomatoes or melons. All year fodder consists
86 of alfalfa, which is cut up to 10 times a year for food. Typical summer crops for fodder are
87 sorghum and Rhodes grass, which is perennial, but dormant in winter. The shallow alluvial
88 aquifers could not sustain the high groundwater abstraction rates for a long time and groundwater
89 level declined dramatically in most areas. Meteorological features of the area are speckled. Five
90 elements of meteorology are constantly recorded through fixed weather station located within the
91 study area. Temperature varies from 6 °C as minimum temperature to 43 °C as maximum
92 temperature. Relative humidity is mostly stable at 24 %. Solar radiation of average sunrise
93 duration is generally 11 hrs/day. Average wind speed is closer to 13 km/hr and may reach up to
94 46 km/hr in thunderstorm incidents. Finally, mean annual rainfall is about 37.6 mm (Al-Zahrani
95 and Baig, 2011).



96 **Figure 1. Location of the study area (Elhag, 2016).**

97 **2.2. Methodological framework**

98 The current research work is based on assessing a regression correlation between estimated
99 evapotranspiration data conducted from AATSR and MERIS sensors and its corresponding
100 ground truth evapotranspiration data conducted through standardized Penman-Monteith.
101 Therefore, accurate synchronization of remote sensing data bypassing and ground truth data
102 collection were exercised.

103 **2.3. SEBS Model fundamentals**

104 Remote sensing data acquired from Advance Along Track Scanner Radiometer (AATSR) and
105 Medium Spectral Resolution Imaging Spectrometer (MERIS) sensors in the 8th of July 2013
106 respectively. The satellite data were georeferenced to WGS-84 datum, atmospherically corrected
107 using SMAC correction (Rahman and Dedieu, 1994). Several meteorological data collected from
108 a stationary station located within the designated study area (2004-2014, average meteorological
109 data).

110 Surface Energy Balance System was initiated by Su (2002) based on further Surface Energy
111 Balance Index improvements. SEBS dynamicity works for regional and local ET estimation.
112 Regional ET estimation uses Monin–Obukhov Similarity (MOS), Bulk Atmospheric Similarity
113 and thermal roughness principles. On the other hand, local ET estimation uses only Atmospheric
114 Surface Layer (ASL) scaling fundamentals (Brutsaert 1999; Su, 2001, Su et al., 2001). The
115 boundary conditions (wet and dry) are essential components in ET estimation using SEBS
116 model. According to the water availability limitation, H_{dry} is considered to be equal to the
117 available energy AE as evaporation assumed to be “zero”. Following Penman–Monteith



118 parameterization (Monteith 1965, 1981), wet boundary condition (H_{wet}) is calculated as
119 following:

$$120 \quad H_{wet} = AE - \frac{\left(\frac{\rho \alpha c p}{r_{ah}}\right) \left(e_s - \frac{e}{\gamma}\right)}{1 + \frac{\Delta}{\gamma}} \quad (1)$$

121 Where

122 e is the actual vapor pressure (kP_a),

123 e_s is the saturation vapor pressure (kP_a),

124 c is the psychrometric constant ($kP_a \text{ } ^\circ C^{-1}$),

125 γ is the rate of change of saturation vapor pressure with temperature ($kP_a \text{ } ^\circ C^{-1}$) and

126 r_{ah} is the bulk surface external or aerodynamic resistance ($s \text{ } m^{-1}$).

127 Consequently, evaporative fraction (Λ) and relative evaporative fraction (Λ_r) are calculated as
128 following per image pixel:

$$129 \quad \Lambda = \frac{\lambda E}{R_n - G} = \frac{\Lambda_r \lambda E_{wet}}{R_n - G} \quad (2)$$

$$130 \quad \Lambda_r = 1 - \frac{H - H_{wet}}{H_{dry} - H_{wet}} \quad (3)$$

131 Daily evaporation is estimated based on the estimation of the evaporative fraction only when the
132 daily net energy (G) and the net radiation (R_n) are available. Therefore, the amplitude variation
133 of the diurnal energy cycle is sky clarity dependent.

$$134 \quad H = (1 - \Lambda) \cdot (R_n - G) \quad (4)$$

$$135 \quad LE = \Lambda (R_n - G) \quad (5)$$



$$136 \quad E_{daily} = A_0^{24} \cdot \int_{daytime} \frac{R_n - G_0}{\lambda \rho \omega} \quad (6)$$

137 Where

138 A is the evaporative fraction

139 A_r is relative evaporative fraction

140 R_n is net radiation measured in watt per square meter,

141 G is soil heat flux measured in watt per square meter,

142 H is turbulent sensible heat flux measured in watt per square meter,

143 λE is turbulent latent heat flux measured in watt per square meter,

144 H is the actual sensible heat flux and determined by the bulk atmospheric similarity approach.

145 $\rho \omega$ is the density of water measured in kilograms per cubic meter.

146

147 **2.4. Validation**

148 Using standardized Penman-Monteith method, 50 ground truths data collected were collected
149 and used to validate the implemented model. The sampling locations were consistently
150 distributed over the designated study area. The lysimeter technique for the estimation of daily
151 evapotranspiration was carried out following Liu and Wang (1999) with calibrated accuracy
152 equal to ± 0.025 . The calibration procedure was principally based on placing double
153 infiltrometers (Taylor 1981).

154 The corrected Penman equations for estimating the daily evapotranspiration was conducted
155 according to Jensen et al., (1990):

$$156 \quad ET_0 = \left[\frac{\Delta}{\Delta + \gamma} R_n + \frac{\gamma}{\Delta + \gamma} f(U) (e_s - e_a) \right] c \quad (7)$$

157 Where

158 ET_0 is reference evapotranspiration (mm /day),

159 Δ is the slope of saturation vapor pressure-temperature curve (kPa /°C),



160 γ is the psychrometric constant (kPa /°C),

161 R_n is the net radiation (mm (mbar)),

162 c is the adjustment factor,

163 $f(U)$ is the wind function,

164 e_s is the saturation vapor pressure (mbar),

165 e_a is actual vapor pressure,

166

167 Consequently, the wind function was conducted following to Doorenbos and Pruitt (1977) as:

$$168 \quad f(U) = 0.27 \left(1 + \frac{U_2}{100} \right) \quad (8)$$

169 Where

170 U_2 is the wind speed measured surfacely at 2 m height (km/day).

171

172 Meanwhile, e_a was calculated according to Allen et al. (1998) as the following:

$$173 \quad e_a = \frac{e^o(T_{min})(RH_{max}/100) + e^o(T_{max})(RH_{min}/100)}{2} \quad (9)$$

174 Where

175 $e^o(T_{min})$ is the saturation vapor pressure at a daily minimum temperature (kPa),

176 $e^o(T_{max})$ is the saturation vapor pressure at a daily Maximum temperature (kPa),

177 RH_{max} is the maximum relative humidity (%),

178 RH_{min} is minimum relative humidity (%).

179

180 Linear regression model was used to find the correlation coefficient between the estimated and

181 the actual evapotranspiration values. Root Mean Square Error (RMSE) was used to signify the

182 inequality of variance and correlation of the linear regression model (Box, 1954). The R|RMSE

183 was calculated as following:

$$184 \quad RMSE = [N^{-1} \sum_{i=1}^N (P_i - O_i)^2]^{0.5} \quad (10)$$

185 Where



186 N is the number of observations,
187 P_i is the predicted ET values (mm/day)
188 O_i is the calculated ET values (mm/day)

189

190 **3. Results and Discussion**

191 SEBS model implementation over the designated study area results in 10 different turbulent heat
192 fluxes thematic maps. The histogram and the scatter plot of SEBS output thematic maps were
193 plotted against the daily evapotranspiration values. Daily evapotranspiration values ranging from
194 zero to map indicates the range of the actual evapotranspiration in the study area ranges between
195 zero and 6.61 mm/day. The spatial distribution of the highest evapotranspiration area is the
196 peripheral of the agricultural pivots as it's demonstrated in Figure 2. This could be explained by
197 the poor drainage system were the access of irrigational water collated at the sides of the pivots
198 (Zwart and Bastiaanssen, 2004; Cruz-Blanco et al., 2014). The mean actual evapotranspiration
199 value is almost 5 mm/day (Figure 3), which is considered a high value in such arid conditions
200 (Elhag et al., 2011). Such evapotranspiration value supports the hypothesis of the
201 mismanagement of irrigational water in Wadi Ad Dawasir. Principally under extreme dry climate
202 conditions, relative evaporation may reach unity (Lockwood, 1999). The relative evaporation
203 thematic map; demonstrated in Figure 4, confirms high correspondence between the actual and
204 the potential evapotranspiration, especially in the peripheral of the agricultural pivots. Normal
205 distribution of the relative evaporation is demonstrated in Figure 5. Mean relative evaporation
206 ratio is counted for 0.91. Only within the pivots, the relative evaporation decreases to 0.45
207 indicating the wet condition of the agricultural land (De Bruin et al., 2010). 50 points of ground
208 truthing data were collected during July 2013 of daily evapotranspiration. The points were



209 consistently distributed over the designated study area. Daily evapotranspiration estimation was
210 conducted according to Liu and Wang (1999) using the Lysimeter with calibrated accuracy of \pm
211 0.025. The actual evapotranspiration data were intersected with the estimated raster image under
212 GIS environment. A linear regression model with R^2 value of 0.83 was conducted to assess the
213 association between the estimated and the actually measured values (Figure 6).

214 Implementation of SEBS model over the designated study area proved a higher daily
215 evapotranspiration values than projected. Higher daily evapotranspiration values were noticed
216 because the sensible heat flux is the major part of the energy, while the latent heat flux is
217 dominating only over the agricultural area (Frey et al., 2010; Elhag 2014a,b). SEBS model
218 behavior could be explained by the model tendency to simulate the potential daily
219 evapotranspiration rather than the actual daily evapotranspiration, which is identified as the lack
220 of Leaf Area Index value over desert areas (Li, et al., 2009; Elhag et al., 2011). The application
221 of SEBS model over the designated study area showed insignificance difference than the Nile
222 Delta Case in term of accuracy assessment (Elhag et al., 2013).

223

224 **Figure 2. Actual daily evapotranspiration thematic map.**

225

226 **Figure 3. Normal distribution of actual daily evapotranspiration data.**

227

228 **Figure 4. Relative evaporation thematic map.**

229



230 **Figure 5. Normal distribution of relative evaporation data.**

231

232 **Figure 6. The relationship between actual and simulated daily evapotranspiration.**

233

234 **Conclusions**

235 Projected evapotranspiration data using SEBS model and multiple remote sensing imageries
236 demonstrated robust association with the ground truth data. The application of the SEBS model
237 mapped the daily evapotranspiration and evaporative fraction objectively over Wadi Ad Dwaser
238 region. The findings of the current research will help the decision makers towards modification
239 of the agriculture activities in similar areas, in term of conservative irrigational water regulations.
240 The model shows consistent results in the estimation of daily evapotranspiration in Nile Delta
241 region and in Wadi Ad Dwaser. Accordingly, SEBS model can be considered as a reliable
242 effective tool in the estimation of daily evapotranspiration explicitly in arid environments.

243

244 **Acknowledgement**

245 This project was funded by the Deanship of Scientific Research (DSR) at King Abdulaziz
246 University, Jeddah, under grant no. (G-182-155-37). The authors, therefore, acknowledge with
247 thanks, DSR technical and financial support.

248

249 **References**

250 Allen, R. G., Tasumi, M. and Trezza, R. (2007a). Satellite-based energy balance for mapping
251 evapotranspiration with internalized calibration (METRIC) – Model. American Society
252 of Civil Engineers, Journal of Irrigation and Drainage Engineering. 133(4): 380394



- 253 Allen, R. G., Tasumi, M., Morse, A. T., Trezza, R., Kramber, W., Lorite I. and Robison, C. W.
254 (2007b.) Satellite-based energy balance for mapping evapotranspiration with internalized
255 calibration (METRIC) – Applications. American Society of Civil Engineers, Journal of
256 Irrigation and Drainage Engineering. 133(4): 395-406
- 257 Al-Zahrani, K. H. and Baig, M. B. (2011). Water in the Kingdom of Saudi Arabia: Sustainable
258 Management Options. The Journal of Animal and Plant Sciences, 21: 601– 604.
- 259 Bastiaanssen, W. G. M., Pelgrum, H., Wang, J., Ma, Y., Moreno, J., Roerink G. J. and van der
260 Wal, T. (1998b). The Surface Energy Balance Algorithm for Land (SEBAL): Part 2
261 validation, Journal of Hydrology, 212-213.
- 262 Beljaars, A. C. M. and Holtlag, A. A. M. (1991). Flux parameterization over land surfaces for
263 atmospheric models, Journal of Applied Meteorology, 30: 327–341.
- 264 Berengena, J. and Gavilán, P. (2005). Reference evapotranspiration Estimation in a highly
265 advective semiarid environment. American Society of Civil Engineers, Journal of
266 Irrigation and Drainage Engineering, 131(2): 147–163.
- 267 Bernstein, L. S., Adler-Golden, S. M., Sundberg, R. L., Levine, R. Y., Perkins, T. C., Berk, A.,
268 Ratkowski, A. J., Felde, G. and Hoke, M. L. (2005). Validation of the QUick
269 Atmospheric Correction (QUAC) algorithm for VNIR-SWIR multi- and hyperspectral
270 imagery. SPIE Proceedings, Algorithms and Technologies for Multispectral,
271 Hyperspectral, and Ultraspectral Imagery XI. Vol. 5806, pp. 668-678.
- 272 Box, G. E. P. (1954). Some Theorems on Quadratic Forms Applied in the Study of Analysis of
273 Variance Problems, II: Effects of Inequality of Variance and Correlation Between Errors
274 in the Two-Way Classification. Annals of Mathematical Statistics, 1, 69-82.
- 275 Brest, C. L. and Goward, S. N. (1987). Deriving Surface Albedo Measurements from Narrow
276 Band Satellite Data. International Journal of Remote Sensing, 8: 351-367.
- 277 Brutsaert, W. (1982). Evaporation into the atmosphere, Reidel, Dordrecht, 299 pp.
- 278 Brutsaert, W. (1991). The formulation of evaporation from land surfaces. p. 67–84. In D. S.
279 Bowles and P. E. O’Connell (eds.) Recent Advances in the Modeling of Hydrologic
280 Systems. Kluwer Academic Publishers, Boston, MA, USA.



- 281 Brutsaert, W. (1999). Aspects of Bulk Atmospheric Boundary Layer Similarity under Free
282 Convective Conditions. *Reviews of Geophysics*, 37: 439–451.
- 283 Cammalleri, C. and Ciraolo, G. (2013). A simple method to directly retrieve reference
284 evapotranspiration from geostationary satellite images. *International Journal of Applied*
285 *Earth Observation and Geoinformation*, 21: 149–158.
- 286 Chávez, J. L., Neale, C. M. U., Hipps, L. E., Prueger, J. H., and Kustas, W. P. (2005).
287 Comparing aircraft-based remotely sensed energy balance fluxes with eddy covariance
288 tower data using heat flux source area functions. *Journal of Hydrometeorology*, 6(6):
289 923–940.
- 290 Crago, R. and Crowley, R. (2005). Complementary relationship for near instantaneous
291 evaporation. *Journal of Hydrology*, 300: 199–211.
- 292 Cristobal, J. and Anderson, M. C. (2012). Regional scale evaluation of a MSG solar radiation
293 product for evapotranspiration modeling. *Hydrology and Earth System Sciences*, 9:
294 8905–8939.
- 295 Cruz-Blanco, M., Gavilán, P., de Bruin, H. A. R., Trigo, I. F., Santos, C. and Lorite, I. J. (2014).
296 Reference evapotranspiration assessment using remote sensing and forecasting tools
297 under semi-arid conditions. *International Journal of Applied Earth Observation and*
298 *Geoinformation*, 33: 280–289.
- 299 De Bruin, H. A. R., Trigo, I. F., Jitan, M. A., Temesgen, E. N., van der Tol, C. and Gieske, A. S.
300 M. (2010). Reference crop evapotranspiration derived from geo-stationary satellite
301 imagery: a case study for the Fogera flood plain, NW-Ethiopia and the Jordan Valley.
302 *Jordan. Hydrology and Earth System Sciences*, 14: 2219–2228.
- 303 Elhag, M. (2016). Evaluation of Different Soil Salinity Mapping Using Remote Sensing
304 Techniques in Arid Ecosystems, Saudi Arabia. *Journal of Sensors*, 2016: 96175-96175.
- 305 Elhag, M. (2014b). Sensitivity Analysis Assessment of Remotely Based Vegetation Indices to
306 Improve Water Resources Management. *Environment Development and Sustainability*,
307 16(6): 1209-1222.



- 308 Elhag, M. (2014a). Remotely Sensed Vegetation Indices and Spatial Decision Support System
309 for Better Water consumption Regime in the Nile Delta. A Case Study for Rice
310 Cultivation Suitability Map. *Life Science Journal*, 11(1): 201-209.
- 311 Elhag, M., Psilovikos, A., Manakos, I., Perakis, K. (2011). Application of the SEBS Water
312 Balance Model in Estimating Daily Evapotranspiration and Evaporative Fraction from
313 Remote Sensing Data over the Nile Delta. *Water Resources Management*, 25(11): 2731 -
314 2742.
- 315 Espadafor, M., Lorite, I. J., Gavilán, P. and Berengena, J. (2011). An analysis of the tendency of
316 reference evapotranspiration estimates and other climate variables during the last 45
317 years in Southern Spain. *Agricultural water management*, 98: 1045–1061.
- 318 Gavilán, P., Lorite, I. J., Tornero, S. and Berengena, J. (2006). Regional calibration of
319 Hargreaves equation for estimating reference ET in a semiarid environment. *Agricultural
320 water management*, 81: 257–281.
- 321 Ghilain, N., Arboleda, A. and Gellens-Meulenberghs, F. (2011). Evapotranspiration modelling at
322 large scale using near-real time MSG SEVIRI derived data. *Hydrology and Earth System
323 Sciences*, 15: 771–786.
- 324 Hanson, R. L. (1991). "Evapotranspiration and Drought." In: *National Water Summary 1988-89-
325 -Hydrologic Events Floods and Droughts*. R.W. Paulson, E.B. Chase, R.S. Roberts and
326 D.W. Moody (eds.). USGS, Water-Supply paper 2375, 99-104.
- 327 Lockwood, J. G. (1999). Is Potential Evapotranspiration and Its Relationship with Actual
328 Evapotranspiration Sensitive to Elevated Atmospheric CO₂ Levels?. *Climatic Change*,
329 41(2): 193-212.
- 330 Loheide, S. P. and Gorelick, S. M. (2005). A local-scale, high-resolution evapotranspiration
331 mapping algorithm (ETMA) with hydroecological applications at riparian meadow
332 restoration sites. *Remote Sensing of Environment*, 98: 182–200.
- 333 Psilovikos, A. and Elhag, M. (2013). Forecasting of Remotely Sensed Daily Evapotranspiration
334 Data over Nile Delta Region, Egypt, *Water Resources Management*, 27(12): 4115-4130.
- 335 Rahman, H. and Dedieu, G. (1994). SMAC: a simplified method for the atmospheric correction
336 of satellite measurements in the solar spectrum. *Remote Sensing*, 15(1): 123-143.

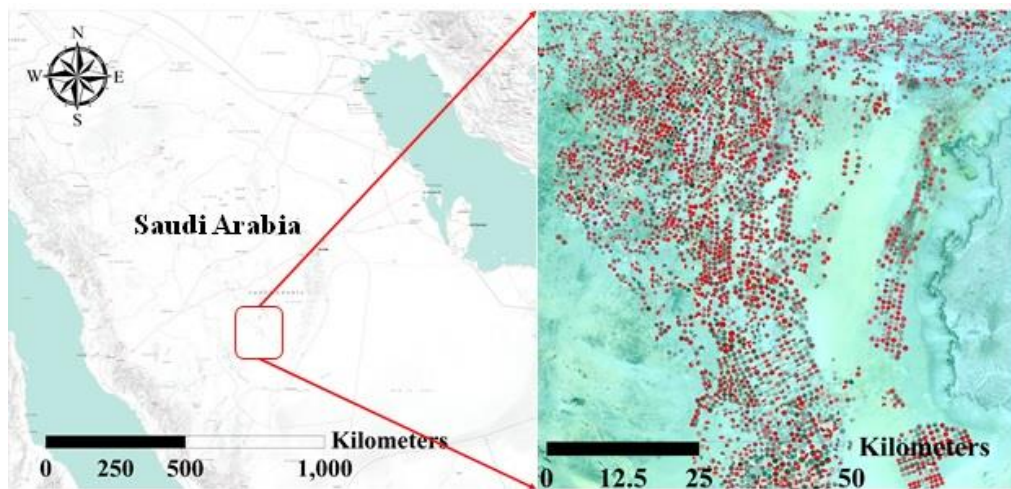


- 337 Roerink, G. J., Su, Z., and Menenti, M. (2000). A simple remote sensing algorithm to estimate
338 the surface energy balance. *Physics and Chemistry of the Earth*, 25: 147–157.
- 339 Su, W., Bodas-Salcedo, A., Xu, K-M. and Charlock, T. P. (2010). Comparison of the tropical
340 radiative flux and cloud radiative effect profiles in a climate model with Clouds and the
341 Earth's Radiant Energy System (CERES) data. *Journal of Geophysical Research*, 115:
342 D01105.
- 343 Su, Z. (2001). A surface energy balance system (SEBS) for estimation of turbulent heat fluxes
344 from point to continental scale. In: Su, Z., Jacobs, C. (eds) *Advanced earth observation
345 land surface climate*. Publications of the National Remote Sensing Board (BCRS), USP-
346 2, 01-02, pp 184–185.
- 347 Su, Z. (2002). The surface energy balance system SEBS for estimation of turbulent heat fluxes.
348 *Hydrology and Earth System Sciences*, 6(1):85–99.
- 349 Su, Z., Schmugge, T., Kustas, P. and Massman, J. (2001). An evaluation of two models for
350 estimation of the roughness height for heat transfer between the land surface and the
351 atmosphere. *Journal of Applied Meteorology*, 40(11):1933–1951.
- 352 Su, Z., Yacob, A., Wen, J., Roerink, G., He, Y., Gao, B., Boogaard, H. and Diepen, C. (2003).
353 Assessing relative soil moisture with remote sensing data: theory, experimental
354 validation, and application to drought monitoring over the North China Plain. *Physics and
355 Chemistry of the Earth*, 28:89–101.
- 356 Tasumi, M., Trezza, R. and Allen, R.G., 2006. *METRIC Manual for MODIS Image Processing
357 Version 1.0 (April, 2006)*. University of Idaho R&E Center, Kimberly, Idaho. 67 p.
- 358 Van den Hurk, B. J. J. M and Holtslag, A. A. M. (1995). On the bulk parameterization of surface
359 fluxes for various conditions and parameter ranges; *Boundary-Layer. Meteorology* 82:
360 199-B4.
- 361 Zwart, S. J. and Bastiaanssen, W. M. G. (2004). Review of measured crop water productivity
362 values for irrigated wheat, rice, cotton and maize. *Agricultural Water Management*, 69:
363 115–133.
- 364



365

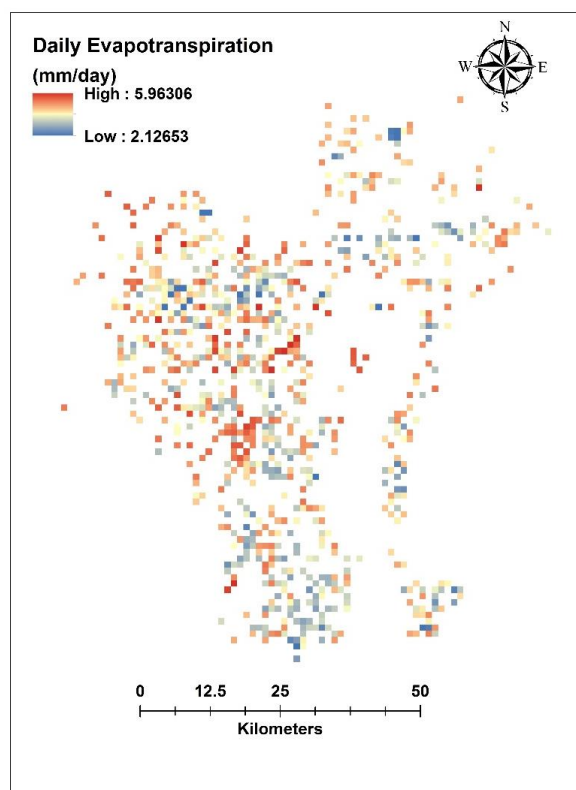
List of figures



366

367

Figure 1. Location of the study area (Elhag, 2016).



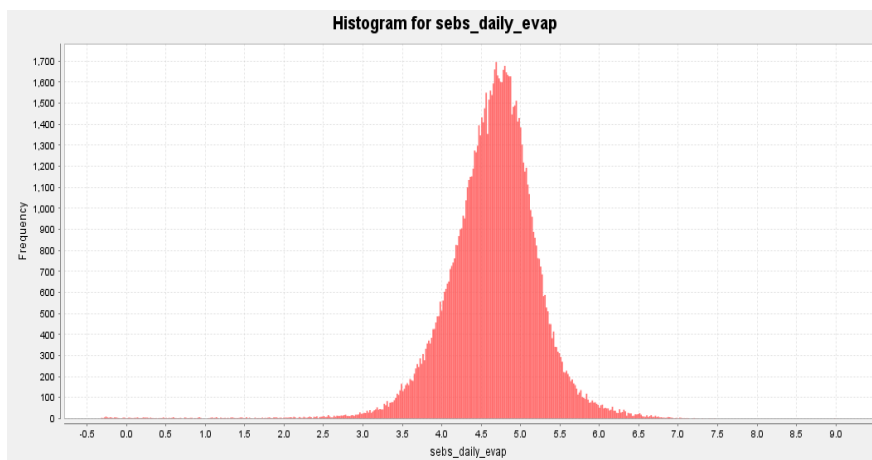
368

369

Figure 2. Actual daily evapotranspiration thematic map.

370

371



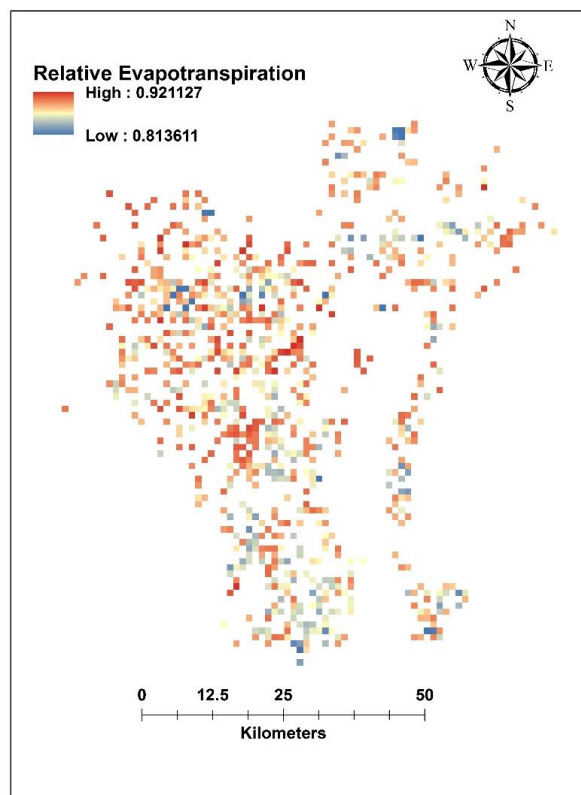
372

373

Figure 3. Normal distribution of actual daily evapotranspiration data.

374

375



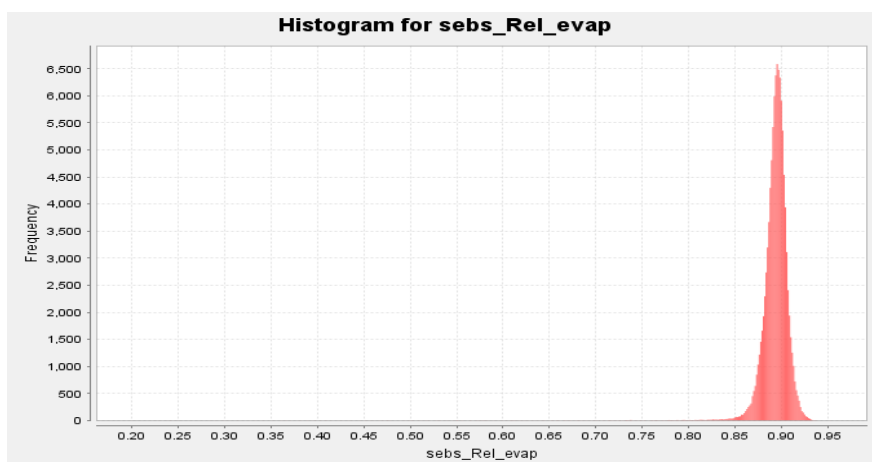
376

377

Figure 4. Relative evaporation thematic map.

378

379



380

381

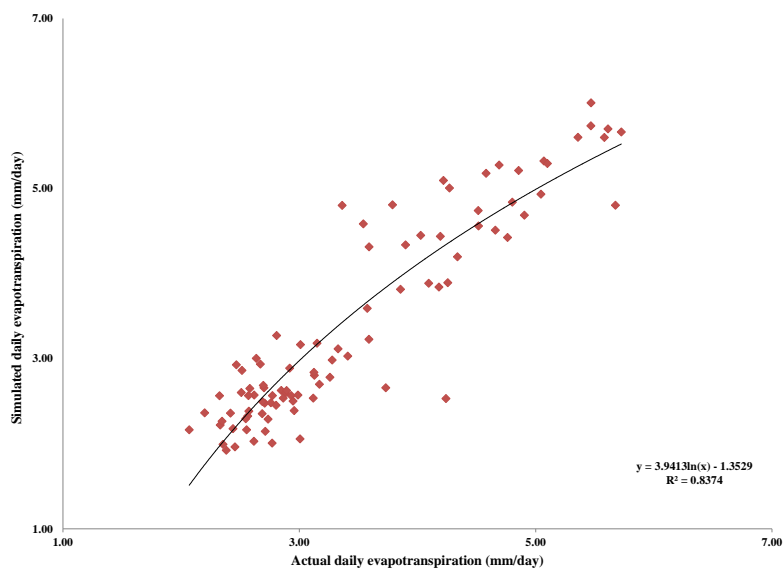
Figure 5. Normal distribution of relative evaporation data.

382

383

384

385



386

387

388

Figure 6. The relationship between actual and simulated daily evapotranspiration.